Article

Optimization, Kinetics, and Isotherm Studies of Methyl Thioninium Chloride Removal from Simulated Solutions Using Chitosan Derivatives

Manar El-Sayed Abdel-Raouf, Reem Kamal Farag, Ahmed A. Farag,* Mohamed Keshawy, Alaa Abdel-Aziz, and Abdulraheim Hasan

Read Online

ACCESS | Metrics & More | Article Recommendations

ABSTRACT: Methylene blue (MB) dye or methyl thioninium chloride is one of the hazardous cationic dyes that are discharged into the textile effluent causing a highly negative environmental impact. The present work targets the investigation of the adsorption performance of some chitosan-modified products toward the MB dye from simulated solutions. The claimed chitosan derivatives were prepared, characterized, and applied for the removal of lead and copper cations from an aqueous medium in a previous work. These include: N,O-carboxymethyl chitosan (N,O-CM/Cs), chitosan grafted with glutaraldehyde (Cs/GA), chitosan cross-linked with GA/epichlorohydrin (Cs/GA/ECH), and chitosan cross-linked with glutaraldehyde/methylene bis(acrylamide) (Cs/GA/MBA). The modified chitosan derivatives in this study displayed outstanding mechanical qualities, exceptional reusability, and

a significant amount of adsorption capacity. The ability of prepared Cs derivatives to eradicate MB was as follows: N,O-CM/Cs (95.1 mg/g) < Cs/GA (120.1 mg/g) < Cs/GA/ECH (220.1 mg/g) < Cs/GA/MBA (270.0 mg/g). The swelling performance of the prepared sorbents was verified under different experimental conditions, and the data revealed that the maximum swelling was attained at pH = 9, temperature 55 °C, and after 24 h. The produced Cs derivatives showed exceptional reusability by maintaining higher adsorption effectiveness throughout five cycles. The MB dye was adsorbed onto the modified derivatives according to pseudo-second-order kinetics and the Langmuir model. Moreover, the adsorption process was monitored via atomic force microscopy to verify the differences between the dye-free and dye-loaded adsorbents.
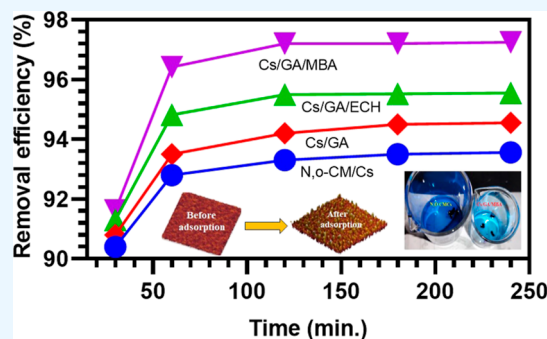
1. INTRODUCTION

The extraordinary growth of the textile industry has resulted in a huge increase in the demand for organic dyestuffs as primary colorants. The yearly global production of dyes was anticipated to surpass 700,000 tons until recently.[1−4] Yet, 15−20% of all the dyestuffs used in this industry were discharged into bodies of water.[5,6] Methylene blue (MB), one of the most often utilized cationic dyes, possesses a high color saturation that blocks sunlight from penetrating water bodies, hindering photosynthesis in aquatic creatures, and posing a serious threat to the ecological balance of water bodies.[7,8] When taken after an inappropriate exposure, MB can also cause respiratory distress, diarrhea, vomiting, and other unpleasant symptoms.[9,10] To protect the environment and public health, dyes must be removed from wastewater.[11] The treatment of printing and dyeing wastewater using conventional technologies includes membrane filtration,[12] adsorption,[13,14] chemical oxidation,[15] photodegradation,[16] etc. Adsorption has been the method of choice for the treatment of dyeing wastewater because of its simplicity, high efficacy, wide applicability, cheap operating costs, and environmental friendliness.[17−19] Due to its ease of

chemical modification and chemical stability, chitosan is a typical representative of biomass-based absorbents. Chitosan is an abundant supply of amino and hydroxyl groups that can use electrostatic and hydrogen bonding to absorb dyes and heavy metal ions.[20,21] It is the second most abundant renewable natural resource after cellulose.[22] On the other hand, chitosan possesses some drawbacks, which restrict its application in neat form such as weak mechanical qualities, a limited specific surface area, and ease of acid dissolution.[23,24] It can be typically altered through procedures including cross-linking,[25] grafting,[26] the addition of magnetic species,[27] and nanoparticles,[28] by chemical protocols,[29] and gamma irradiation[30] before being widely employed in a range of wastewater treatment treatments. Several chitosan-

modified products have been employed in the removal of different pollutants from aqueous solutions. In this regard, Chandra et al.[31] investigated sodium tripolyphosphate and vanillin-modified chitosan-based magnetic nanosorbents for removal of different heavy metal cations from aqueous solutions. Moreover, magnetic β-cyclodextrin−chitosan/graphene oxide was employed in the removal of MB with an efficiency of about 84.3 mg/g.[32] In addition, Li et al.[33] prepared chitosan-coated magnetic mesoporous silica nanoparticles as sorbents. On the other hand, in the presence of certain agents such as glutaraldehyde (GA) and epichlorohydrin (ECH), chitosan chains can be chemically cross-linked to create triple network architectures with enhanced mechanical and adsorption capabilities.[34] This research article focuses on the functionalization of chitosan modified from shrimp shell chitin using carboxymethylation, grafting with GA, cross-linking with ECH, and with methylene bis(acrylamide) (MBA) (as per our previous work[34]) to create reasonably priced sorbents for the removal of MB from aqueous environments. The kinetics of the removal process and the adsorption isotherms were carefully examined, and the produced derivatives were fully described by using a variety of techniques. Also, the experimental variables that impact the dye uptake mechanism were thoroughly investigated. One of the material's advantages and innovations is the use of four modified chitosan products including cross-linked and non-cross-linked chitosan as a set of green polymers in comparative research for eliminating MB dye. In addition, the adsorption process was confirmed by atomic force microscopy (AFM) by comparing the height and surface topographies of dye-free and dye-loaded samples.

2. MATERIALS AND METHODS

2.1. Materials. Chitin from shrimp shells was converted to chitosan with an 88% degree of deacetylation and an M_w of about $1-3 \times 10^5$ g/mol. Chloroacetic acid was supplied from Sigma-Aldrich as high-purity white crystals. Glacial acetic acid, an ultrapure colorless liquid with a strong odor, was available at Sigma-Aldrich—Germany. Other chemicals including ketoglutaric acid (analytic reagent fine white powder), hydrochloric acid (37%), sodium borohydride as white powder of 98% purity, glutaraldehyde (GA) with 50 wt % in DW, and epichlorohydrin (ECH) as colorless liquid were all obtained from El-Nasr Company for Chemicals (Local Supplier). Methylene bis-(acrylamide) (MBA) is a light-colored crystal that was purchased from Thermo Fisher in the United States.

2.2. Uncross-linked Chitosan Adsorbent Preparation.[34] Shortly, 5 g of chitosan (Cs) was well dissolved in 100 mL of 1% acetic acid solution. The pH was then adjusted to roughly 5.0 with NaOH solution while rapidly stirring for 4 h at room temperature with the gradual addition of 8 g of ketoglutaric acid. The pH was then adjusted to neutral with drops of 1 N HCl solution, and the process was allowed to run for 12 h. Finally, the product was separated, filtered, and washed with ethanol before being transported to a Soxhlet extractor and continuously extracted with ethanol for 6 h. After vacuum drying, the dried solid N,O-carboxymethyl chitosan (N,O-CM/Cs) was produced. On the other hand, 2 g of Cs in solution was put into a precipitation bath containing 500 mL of 0.50 M NaOH with continuous stirring to make Cs/GA beads. During an hour, the necessary amount of GA was added while constantly stirring. The wet chitosan gel beads were thoroughly rinsed with distilled water to eliminate any NaOH, then filtered and air-dried to remove the water from the pore structure to

obtain chitosan beads. Before usage, the beads were crushed and sieved to an average size of <250 μm.

2.3. Preparation of Cross-linked Chitosan Adsorbents.[34] Freshly prepared wet Cs/GA beads were heated to 45 °C and then mixed in a cross-linker solution (pH = 10) comprising 0.2 M equal molar ratio of GA/ECH or GA/MBA and then stirred for 2 h. The cross-linked beads were filtered and thoroughly rinsed with distilled water to eliminate any unreacted cross-linkers, before being filtered and air-dried. Before usage, the newly produced products (Cs/GA/ECH and Cs/GA/MBA) were crushed and sieved to a consistent size (<250 μm).

2.4. Preparation of MB Solution. A dye stock solution was made by dissolving 1 g of the MB in 1 L of distilled water. The prepared stock was kept in a refrigerator before the adsorption test. To create solutions at different concentrations that were used in the investigations, the stock solution was diluted.

2.5. Swelling Ability. The swelling capacity of chitosan sorbents in different media was evaluated by dipping 0.02 g of each dry sample in 20 mL of various buffer solutions (pH 4, pH 7, and pH 9) at different temperatures (25, 35, and 55 °C) in a static position overnight. The swollen sample was removed from the medium, gently wiped with filter paper to remove the droplets on its surfaces, and reweighed. Its swelling capacity was calculated according to eq 1.[35]

$$\text{Swelling capacity (\%)} = \left(\frac{W_0 - W_1}{W_0} \right) \times 100 \tag{1}$$

where W_0 and W_1 are the weights of the dry and swelled samples, respectively. Swelling measurements were taken as the average of three comparable results.

2.6. Removal Performance Experiments. The adsorption capacities and the rate of clearance of the MB dye achieved by the produced adsorbents were thoroughly assessed. This was conducted by mixing 0.05 g of chitosan-modified adsorbents with 50 mL of MB solution (100−400 mg/L). Then, 1 mL of the solution was withheld from the solution at regular intervals to measure the amount of dye still present after adsorption using an atomic absorption spectrometer. The following formulas were used to calculate the MB percentage removal (R %) and the amount adsorbed at equilibrium (q_e)

$$R\ (\%) = \frac{C_o - C_e}{C_e} \times 100 \tag{2}$$

$$q_e = \frac{(C_o - C_e) \times V}{m} \tag{3}$$

where C_0 and C_e are the dye's initial and equilibrium concentrations (mg/L), respectively. The volume of MB solution by the liter, denoted by the symbol V, and the mass of the adsorbent in grams, denoted by the symbol m. The dye concentration was varied from 100 to 400 mg/L at 25 °C for the batch adsorption isotherm investigations. The uptake experiments were carried out in a pH range of 4−10 and at a temperature range of 25−45 °C to confirm the impact of application circumstances on the effectiveness of the MB removal. Each experiment was carried out three times, with the mean result taken into account. In the present work, four isotherm adsorption models: Langmuir, Freundlich, Temkin, and D−R were analyzed.

2.7. Kinetic Studies. The kinetics of MB dye adsorption onto chitosan sorbents were analyzed by four kinetic models: pseudo-first-order, pseudo-second-order, intraparticle diffusion,

and Elovich models. A full description of these models is given in the Results and Discussion section.

2.8. Regeneration Experiments. The reusability investigation for chitosan-based sorbents was conducted by immersing the adsorbent in 20 mL of ethanol as a desorption medium at pH 7 and 25 °C. The amount of the desorbed dye was calculated using eq 4

$$\text{Dye desorption (\%)} = \left(\frac{q_{\mathrm{d}}}{q_{\mathrm{a}}}\right) \times 100 \tag{4}$$

where q_{d} is the amount of MB dye desorbed from the dye-saturated adsorbent (mg·g), and q_{a} is the amount of the dye adsorbed onto the adsorbent surface (mg·g).

2.9. Characterization of the Green Adsorbents. The prepared adsorbents were characterized as per our previous works.[30,35] Normally, AFM (Flexaxiom Nanosurf, C3000) was used to monitor the process of dye uptake. The scanning electron microscopy (SEM) images of the adsorbent-free and dye-loaded adsorbents are given for Cs/GA/MBA as the best adsorbent.

3. RESULTS AND DISCUSSION

3.1. Factors Affecting Swelling Capacity. The swelling capacity of the sorbent material is a very important property that judges its performance. It is mainly affected by the chemical nature of the architect besides two other external factors, namely, the pH and the temperature of the medium. The data for the effect of these variables on the swelling capacity of the chitosan sorbents are collected in Table 1. Initially, all the data

Table 1. Effect of Temperature and pH on the Swelling Capacity for Chitosan-Based Sorbents (Maximum Swelling Was Attained after 24 h)

sample	swelling capacity, %		
	temperature (°C)	pH	
		4	7	9
N,O-CM/Cs	25	703.4	725.3	768.2
	35	812.7	834.4	877.6
	55	802.9	818.1	855.3
Cs/GA	25	744.2	765.8	789.1
	35	781.4	802.6	831.4
	55	763.5	785.3	799.0
Cs/GA/MBA	25	822.8	875.6	903.2
	35	843.1	884.2	917.3
	55	854.2	904.1	923.6
Cs/GA/ECH	25	811.7	834.7	878.9
	35	824.6	857.4	892.3
	55	841.2	866.8	903.2

can be discussed based on the ability of the architect to combine water molecules at a certain condition. Thus, it is observed that under the same conditions, the swelling capacity increases in the order Cs/GA/MBA > Cs/GA/ECH > Cs/GA > N,O CMCs. This observation could be due to the cross-linking technique creating more voids, which extends the adsorptive areas and increases the removal effectiveness of MB dye. This in turn had an impact on the modified chitosan's surface area, which was discovered to be 22.4, 31.6, 51.6, and 68.9 m²/g for N,O CMCs, Cs/GA, Cs/GA/ECH, and Cs/GA/MBA, respectively.[34] On the other hand, it can be noticed that the maximum swelling

capacity was attained at pH = 9 due to the attraction between the −OH groups and the protons of the amine groups existing within the molecule.

The increment in the swelling capacity may also be ascribed to the free water content, which has high mobility and resulted in the capillary wetting of interconnected open hydrogel pores, which finally causes higher swelling capacity in alkaline media.[1] On the other hand, the effect of temperature on the % swelling capacity can be observed in two different behaviors:

- A linear increase with temperature under all the examined pH values: this behavior is noticed for the cross-linked products (Cs/GA/MBA and Cs/GA/ECH). It can be explained by the expansion of the gel matrix by raising the temperature.[36] This insight is helpful since cross-linked products (Cs/GA/MBA and Cs/GA/ECH) may absorb the MB dye even at higher temperatures.

- An increment when the temperature is raised from 25 to 35 °C due to improvements in the mobility of the generated ions and, consequently, increasing their electrostatic interactions with water molecules. Then, an observed reduction in the % swelling capacity occurs when the temperature increases from 35 to 55 °C. This behavior may be attributed to the detachment of the adsorbed water molecules due to increased kinetic mobility leading to the overall drop.[37]

3.2. Adsorption Parameter Optimization. The effects of the adsorption medium pH, initial dye concentrations, and contact time on the adsorption effectiveness of various adsorbents were carefully examined.

3.2.1. Effect of the Adsorption Medium pH. Due to its direct effect on the protonation of the functional groups in the sorbent material and its influence on its degree of ionization, the pH of the medium is an important factor in determining dye uptake. Batch mode tests in a range of 4−10 confirmed the influence of pH, keeping all of the other factors constant (0.05 adsorbent, 300 ppm of the MB, ambient temperature, and 300 min of contact time). The highest uptake values as shown in Figure 1a were achieved at pH 9 for all the investigated compounds. This is due to the low decolorization efficiency before and after this pH (9.0), which was discovered by Zango et al.[1] In another work conducted by Labidi et al.,[36] they found that the maximum adsorption of MB dye onto chitosan-*graft*-polyacrylamide was attained at pH = 8. This finding agrees with the previous finding where the maximum swelling was also achieved at pH = 9. When the pH changes from acidic to alkaline, the amount of MB adsorbed by N,O-CM/Cs, Cs/GA, Cs/GA/ECH, and Cs/GA/ MBA adsorbents gradually increases. The electrostatic effect is crucial in the adsorption behavior of MB.[1] Plenty of protons exist in the aqueous solution under acidic circumstances. These protons will increase the positive charge on the surface of the adsorbents, preventing the cationic dye MB from making contact with the active adsorption sites on the surface of the N,O-CM/Cs, Cs/GA, Cs/GA/ECH, and Cs/GA/MBA. When the pH of the solution rises, the adsorbents gradually acquire a negative charge, indicating that hydroxide ions facilitate MB adsorption. Based on the aforementioned experimental results, the arrangement based on adsorbent uptake efficiency was: N,O-CM/Cs < Cs/GA < Cs/GA/ECH < Cs/GA/MBA.

3.2.2. Influence of Initial Dye Concentration. The dye's adsorption onto adsorbents was investigated at various starting concentrations. According to Figure 1b, when the starting concentration was increased from 25 to 100 ppm (mg/L), the
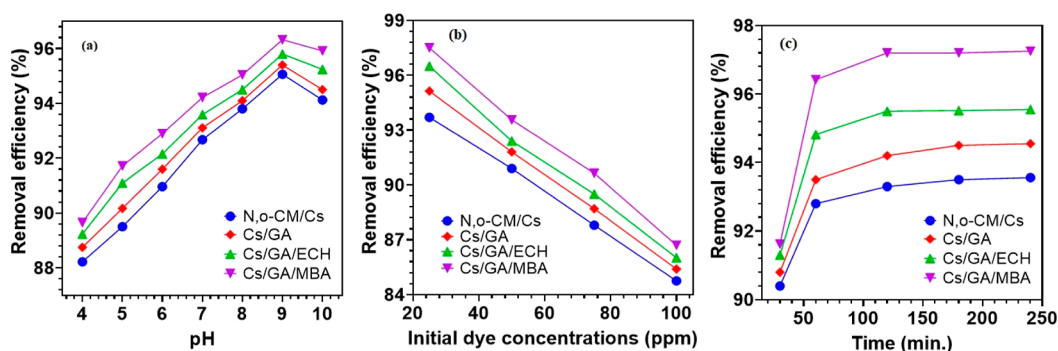
Figure 1. Influences of removal efficiencies of the adsorbents with (a) pH, (b) initial dye concentrations, and (c) contact time.
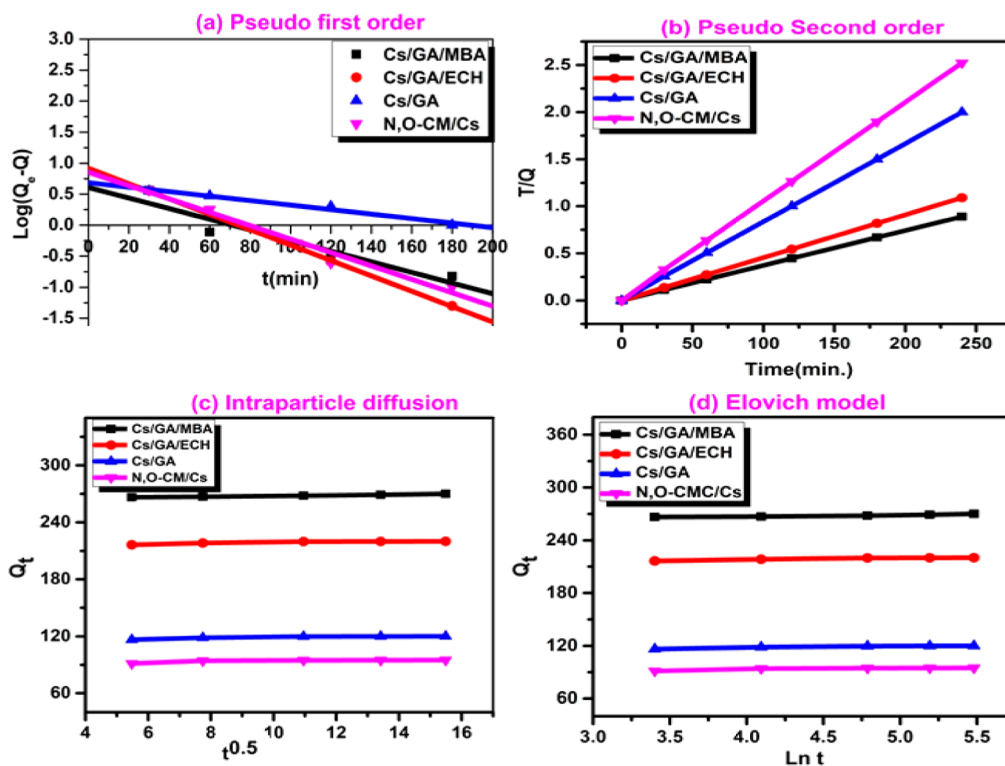

Figure 2. Adsorption kinetics for MB dye onto chitosan-based sorbents at 300 ppm. (a) pseudo-first-order, (b) pseudo-second-order, (c) intraparticle diffusion, and (d) Elovich model.

adsorption efficiency of all of the adsorbents dropped. The examined adsorption efficiency was in the following order: *N,O*-CM/Cs < Cs/GA < Cs/GA/ECH < Cs/GA/MBA, indicating the availability of many active sites on Cs/GA/MBA cross-linked chitosan accessible for MB absorption at high concentrations. The decrease in adsorption efficiency at higher adsorbate concentrations was attributed to a restricted number of adsorption sites accessible for dye uptake. Adsorption ceased as the adsorption sites got saturated. Due to the mass driving force that permits the transport of the dye molecules to the active sites of the adsorbents, the adsorption capacity increased when the initial concentration of the dye was raised.[37]

3.2.3. Effect of Contact Time. The most important factor in the adsorption process is the time of contact between the adsorbent and the adsorbate.[35] Hence, it was examined how contact duration affected the dye's ability to bind to *N,O*-CM/Cs, Cs/GA, Cs/GA/ECH, and Cs/GA/MBA adsorbents. Increased adsorption capacity with contact duration is depicted in Figure 1c. This could be explained by the diffusion of dye

molecules from the solution's surface to the adsorbents' surface. However, over time, the adsorption capacity decreases, most likely as a result of dye molecules moving into the adsorbents' interior pores. The equilibrium was reached after 150 min, and the efficiency was as follows: *N,O*-CM/Cs < Cs/GA < Cs/GA/ECH < Cs/GA/MBA. This indicates that the Cs/GA/MBA cross-linked chitosan has a large number of active sites that are more readily available for MB absorption than other adsorbents.[38] The high adsorption capacity of chitosan-modified products toward MB dye may also be attributed to their high swelling ability, which facilitates the diffusion of dye molecules into the pores of the network. Then, the dye molecules can attach firmly to the inner surface of the sorbent materials through hydrophilic and electrostatic interactions.

3.3. Adsorption Kinetics. *3.3.1. Adsorption Kinetics of the Chitosan-Modified Products toward MB Dye.* The kinetics of the dye uptake process was thoroughly studied to evaluate the typical mechanism and the efficiency of the process.[39] Four adsorption kinetics were used to describe the adsorption of MB

onto the chitosan-modified products at 25 °C and pH 7. The pseudo-first-order, pseudo-second-intraparticle diffusion, and Elovich models are presented in Figure 2, and the kinetic parameters are summarized in Table 2. The mathematical expressions for these models are given in eqs 5−8, respectively.

$$\log(q_e - q_t) = \log q_e - \frac{k_1}{2.303}t \tag{5}$$

$$\frac{t}{q_t} = \frac{1}{k_2 q_e^2} + \frac{t}{q_e} \tag{6}$$

where t is the time (min), q_e, q_t, and q_e^2 are the amounts of water adsorbed onto the adsorbent at equilibrium, at time t, and the maximum adsorption capacity (mg/g), respectively. Also, k_1 and k_2 are the adsorption rate constants of pseudo-first-order (1/min) and pseudo-second-order (g/mg/min).

$$q_t = (K_p t^{1/2}) + C_i \tag{7}$$

where K_p (mg g^{-1} min$^{-1/2}$) is the intraparticle diffusion constant and C_i is the boundary layer thickness. By plotting a linear relation between q_t versus $t^{1/2}$, the values of K_p and C_i can be obtained by slope and intercept calculations, respectively.

3.3.1.1. Elovich Model. This kinetic model can be expressed by eq 8

$$q_t = (1/\beta) \ln(\alpha\beta) + 1/\beta \ln t \tag{8}$$

where α (mg g^{-1} min^{-1}) is the initial rate constant of adsorption, β (g/mg) is the constant of desorption associated with the surface coverage and the activation energy of chemical adsorption, and q_t (mg/g) is the amount of adsorbed dye at time t (min). Both α and β values can be obtained by plotting q_t versus $\ln t$.[40]

Upon dye adsorption, the data given in Table 2 reveal that N,O-CM/Cs, Cs/GA, Cs/GA/ECH, and Cs/GA/MBA follow the pseudo-second order with high R^2 (0.999); i.e., the values tend to unity and the highest adsorption capacity belongs to Cs/GA/MBA among other products with $q_e = 270$ mg/g versus MB dye, which means that the reaction depends only on concentration of two reactants and the adsorption process follows chemisorption type which occurs upon adsorption of MB dye onto chitosan-modified products. This finding infers that the adsorption process is merely a chemisorption, indicating that the rate-limiting step for the adsorption of MB dye onto chitosan sorbents involved an ion exchange process between the cationic dye and the functional groups in the sorbent materials.[2] This outcome runs parallel to Pam et al. in their recent study for the removal of the MB dye using an iodate-chitosan-assembled composite,[41] and the adsorption of reactive red dye onto cross-linked chitosan-epichlorohydrin biobeads.[42] As in some cases, first-order and pseudo-second-order models are insufficient for identifying the mechanism of dye diffusion and could not indicate all the steps that may be involved in the adsorption process (i.e., external film diffusion, adsorption, and intraparticle diffusion), the intraparticle diffusion model was proposed, as it can provide the essential information about the rate-limiting steps. The interparticle diffusion was defined by Weber and Morris as the rate-controlling factor when the adsorption capacity of a specific adsorbent is a function of the square root of time. As there is only one slope (Figure 2, interparticle diffusion), this indicates that the process of dye adsorption involves macropore diffusion of the dye molecule into the active sites distributed within the sorbent molecules as a major process.

Table 2. Adsorption Kinetic Parameters for MB Dye Removal at 300 ppm

kinetics parameters	Cs/GA/MBA	Cs/GA/ECH	Cs/GA	N,O-CM/Cs
Pseudo-first Order				
k_{1ads} (1/min)	0.008	0.025	0.029	0.020
R^2	0.988	0.987	0.990	0.947
q_e (mg/g)	4.8604	7.1613	8.2758	4.0611
Pseudo-second Order				
k_{2ads} (g/mg/min)	0.009	0.014	0.015	0.017
R^2	0.998	0.994	0.993	0.991
q_e (mg/g)	270.002	220.364	120.335	95.279
Intraparticle Diffusion Model				
K_p (mg g^{-1} min$^{-1/2}$)	0.3532	0.3549	0.3403	0.3080
R^2	0.993	0.918	0.900	0.824
C_i (ppm)	264.364	215.171	115.379	90.846
Elovich Model				
β (g/mg)	0.6024	0.5565	0.5762	0.6238
R^2	0.9684	0.9637	0.9519	0.8894
α (mg g^{-1} min^{-1})	1.6707	1.8123	1.7628	1.6330

Table 3. Experimental and Theoretical Q Values According to the Pseudo-second-Order Isotherm

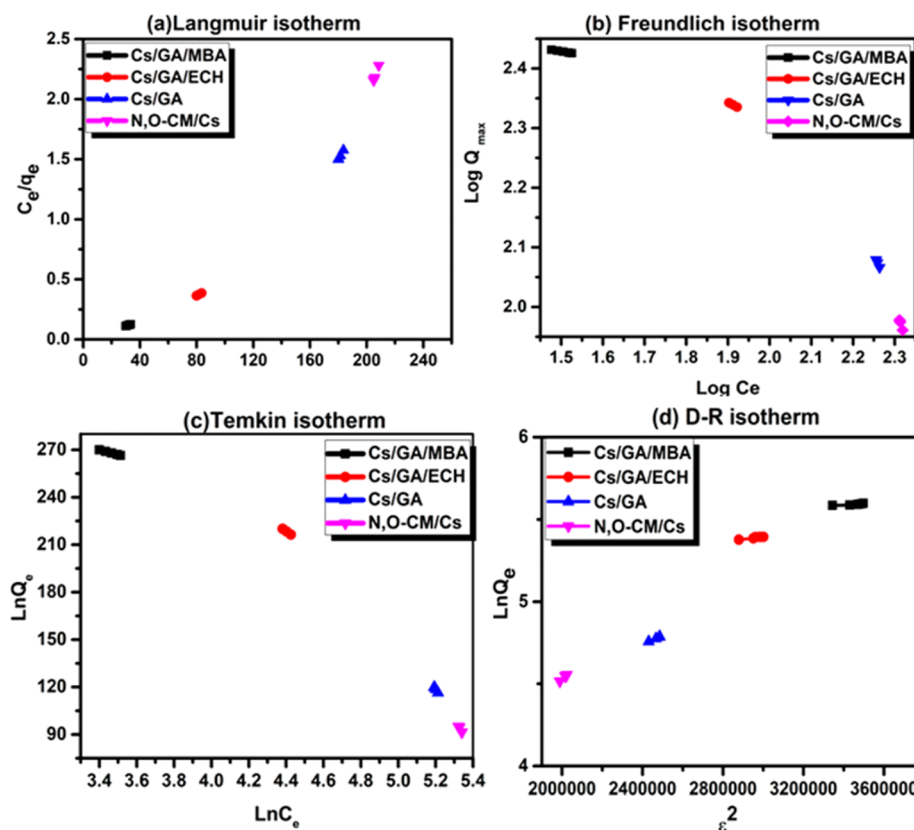| sorbent	$Q_{theo.}$ (mg/g)	$Q_{exper.}$ (mg/g)	sorbent	$Q_{theo.}$ (mg/g)	$Q_{exper.}$ (mg/g)
Cs/GA/MBA	270.002	270.02421	Cs/GA	120.335	120.0705
Cs/GA/ECH	220.364	220.0966	N,O-CM/Cs	95.279	95.0898

Figure 3. Linear adsorption isotherm for the removal of MB dye by chitosan-based sorbents. (a) Langmuir isotherm, (b) Freundlich isotherm, (c) Temkin isotherm, and (d) D−R isotherm.

Similar results were obtained from the adsorption cationic dye on *N,O*-carboxymethyl chitosan.[43] On the other hand, the Elovich model was used on the experimental data using eq 8; the q_t was plotted versus ln t, and the results are illustrated in Figure 2. α and β values, obtained from the plots, are given in Table 2. The validity of the Elovich equation proposes that the adsorption process is governed via the chemisorption mechanism. Moreover, an Elovich model is used to define the second-order model, under the assumption that the solid surface is energetically heterogeneous.[3,43] The experimental data for the adsorption of MB dye onto chitosan sorbents do not agree with the Elovich model. This is ascribed to the low R^2 values, as shown in Table 2.

Thus, the pseudo-second-order kinetic model can more efficiently fit the adsorption of MB dye onto chitosan-based sorbents than the other investigated models. In addition, the calculated values of adsorption capacities, $q_{e,cal}$, resulting from the pseudo-second-order model are close to the experimental adsorption capacities, $q_{e,exp}$ for all of the investigated sorbents as depicted in Table 3.

3.3.2. Adsorption Isotherms of Chitosan-Modified Products. Studying different adsorption isotherms is very important in providing information that describes the reactive interactions between the adsorbate and the adsorbent. Moreover, they provide data about the features of the adsorbing material's surface, the adsorption efficiency, the nature of the adsorbate, and the ongoing adsorption process; whether it is monolayer or multilayer.[44] Also, the adsorption isotherm explores the relationship between the adsorption capacity and concentration at adsorption equilibrium. In this study, four different adsorption isotherms were investigated: Langmuir isotherm equation (9), Freundlich isotherm equation (10), Temkin isotherm equation (11), and Dubinin−Radushkevich isotherm equation (12) models. Figure 3 illustrates the fitting of adsorption isotherm models, while Table 4 lists the equilibrium constants and the corresponding fitting correlation coefficients (R^2).

$$\frac{C_e}{q_e} = \frac{C_e}{q_{max}} + \frac{1}{q_{max}k_l} \tag{9}$$

$$\log q_e = \log k_f + \frac{1}{n} \ln C_e \tag{10}$$

where C_e (mg/L) is the equilibrium concentration, q_e (mg/g) is the equilibrium adsorption capacity, and q_m (mg/L) is the highest saturated adsorption capacity. k_l (L/mg) is the Langmuir adsorption constant related to the adsorption energy, k_f (L/g) is the Freundlich adsorption constant related to the adsorption capacity, and n is the Freundlich constant related to the degree of surface inhomogeneity. On the other hand, the Temkin model is
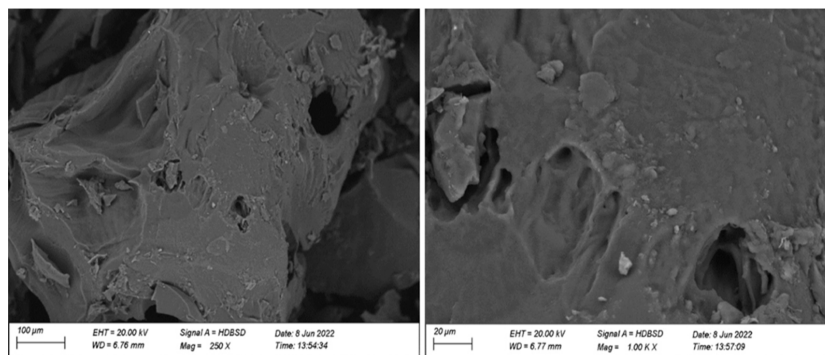
Table 4. Adsorption Isotherm Parameters of the MB Dye at 300 ppm onto Cs/GA/MBA, Cs/GA/ECH, Cs/GA, and N,O-CM/Cs

kinetics parameters	Cs/GA/MBA	Cs/GA/ECH	Cs/GA	N,O-CM/Cs
Langmuir Model				
q_{max} (mg/g)	239.8097	158.8633	46.6230	28.9333
k_l	0.2976	0.0450	0.0091	0.0070
R^2	0.999	0.998	0.996	0.992
Freundlich Model				
n	0.1183	0.3741	1.5364	2.2197
k_f	0.073816	0.047153	0.003910	0.000818
R^2	0.985	0.962	0.941	0.911
Temkin Isotherm				
B_t (J mol^{-1})	31.737	31.434	30.962	30.474
k_t (L/mg)	6.7271×10^{-6}	1.0377×10^{-8}	1.20468×10^{-15}	9.06607×10^{-18}
R^2	0.998	0.987	0.977	0.948
D–R (Dubinin–Radushkevich Isotherm)				
β (mol^2/kJ^2)	7.771×10^{-8}	1.468×10^{-7}	5.504×10^{-7}	1.0914×10^{-6}
ε (kJ/mol)	2536.6124	1845.325448	953.0406295	676.8388191
R^2	0.887	0.955	0.9975	0.9977

another important model that discloses the interaction between the adsorbent and adsorbate. According to this model, adsorption heat decreases linearly upon completing the coverage, and the binding energies are uniformly distributed.

$$q_e = B_t \ln k_t + B_t \ln C_e \tag{11}$$

where B_t (J mol^{-1}) is the Temkin constant that is temperature-dependent, k_t (L/g) is the binding constant of Temkin isotherm, q_e (mg/g) refers to the quantity of dye adsorbed at equilibrium, and C_e (mg/L) is the dye equilibrium concentration at a constant temperature. The values of B_t and k_t constants were obtained from the slope and intercept achieved by plotting q_e against $\ln C_e$.[45]

Dubinin–Radushkevich isotherm is usually applied to differentiate between chemisorption and physisorption. This isotherm fits building up multilayers onto the microporous adsorbents. Thus, this model usually assumes a surface heterogeneity. The D−R isotherm can be expressed as follows

$$\ln q_e = \ln(q_m) - \beta \varepsilon^2 \tag{12}$$

where q_m (mg/g) is the maximum monolayer capacity, β (mol^2 kJ^{-2}) is the activity coefficient, which is dependent on the mean free energy of adsorption per mole of dye when transferred from the bulk of the solution onto the sorbent surface. ε is the Polanyi potential, which can be determined from the following relationship

$$\varepsilon = RT \ln\left(1 + \frac{1}{C_e}\right) \tag{13}$$

where R (8.314 J mol^{-1} K^{-1}) is the universal gas constant and T (K) is the absolute temperature. The values β and $\ln q_m$ in eq 13 can be measured from the intercept and the slope obtained from a plot between $\ln q_e$ versus ε^2, respectively. From the data in Table 4, it is noted that the values of the correlation coefficient (R^2) of the Langmuir isotherm are higher than the other models for all the investigated sorbents. This proves a monolayer adsorption which may be probably due to electrostatic attraction or hydrogen bonding formation between the anionic active sites and the cationic dye. The monolayer adsorption model also discloses the saturation of the active sites with dye molecules after which no further adsorption can take place. Our finding is very close to the findings of Alharby et al.[46] which showed the high applicability of the Langmuir model for the adsorption of MB and dye onto O-CM-chitosan hydrogel. On the other hand, the Freundlich isotherm fits the multilayer adsorption on heterogeneous surfaces.[46] The values of correlation coefficients R^2 are all lower than those calculated for the Langmuir model, confirming the unsuitability of the Freundlich isotherm for the current adsorption processes.

The Temkin isotherm model concerns the connection between the heat of adsorption and the surface coverage. The Temkin parameters β and k_t correspond to the adsorption heat and Temkin isotherm equilibrium binding constant, respectively. It is assumed that the heat of adsorption heat decreased gradually by covering as a result of the reduced interaction between the adsorbent and adsorbate.[45] The lower R^2 values (0.998−0.948) relative to the R^2 values of the Langmuir model revealed the unsuitability of the Temkin model for describing the adsorption of MB dye onto the investigated chitosan sorbents.

Finally, the D−R isotherm is a practical model used to describe the adsorption mechanism for heterogeneous surfaces.

Figure 4. SEM image of Cs/GA/MBA at two magnifications.
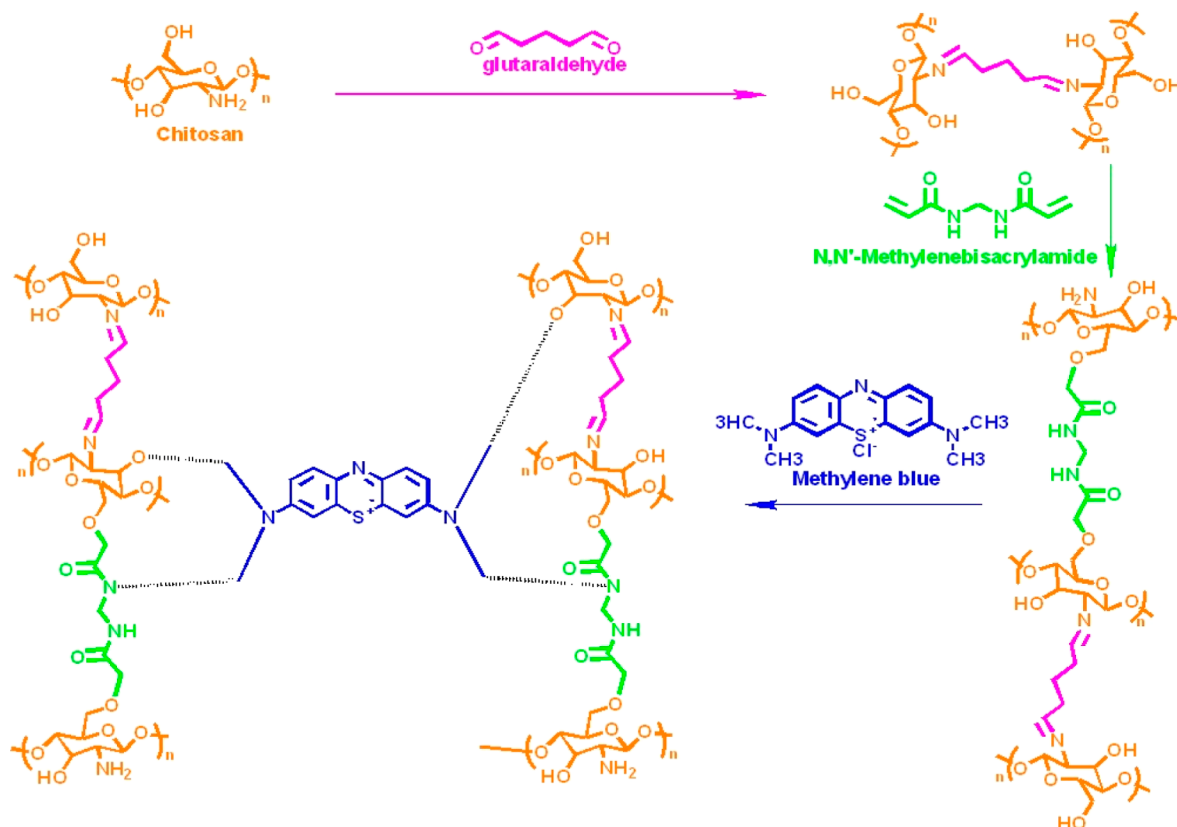

Figure 5. Proposed mechanism of adsorption of MB dye onto chitosan-based sorbents.

This model is only suitable for moderate concentrations of adsorbate, where the adsorption process is controlled by a pore-filling mechanism. As it is temperature-dependent; it can be used to distinguish between physical and chemical adsorption processes. The D−R parameters are illustrated in Table 4. The correlation coefficients R^2 that are displayed in Table 4 confirmed the unsuitability of the D−R isotherm for describing the adsorption of MB dye onto this type of sorbent.

Based on the given correlation coefficient values of R^2, illustrated in Table 4, it can be inferred that the Langmuir isotherm model better fits the experimental data on MB adsorption onto this type of functional chitosan-based sorbents which reflects the surface homogeneity of the prepared sorbents.

3.4. SEM Characterization of Cs/GA/MBA. The morphology of Cs/GA/MBA was confirmed by SEM imaging at two magnifications. The images in Figure 4 reveal a distinct porous

structure that explains the outstanding removal performance of this modified product.

3.5. Mechanism of Adsorption of MB onto the Prepared Sorbents. The present work investigates the adsorption of MB onto four different chitosan-modified products with diverse architects. Therefore, we can expect different adsorption capacities based on various mechanisms. However, the general proposed mechanism is based on attraction between the cationic dye and multiple anionic groups distributed throughout the prepared sorbents. The variation in the quantity of the dye adsorbed onto the sorbent molecule is merely due to differences in the intensity and distribution of these groups throughout the polymeric chain(s). The overall mechanism is given in Figure 5.

3.6. Monitoring the Adsorption of the MB Dye onto the Prepared Sorbents. Figure 6 illustrates the dry and dye-loaded sorbents. It can be noticed that the change in color of the

Figure 6. Free and MB-loaded chitosan-based sorbents.

sorbent material corresponds to its adsorption performance, and the deepest blue color was attained by Cs/GA/MBA which was nominated as the one with maximum adsorption capacity. For comparison, the decolorization of a solution with a 300 ppm MB dye under the optimum conditions by N,O CMCs, and Cs/GA/MBA is given in Figure 7.
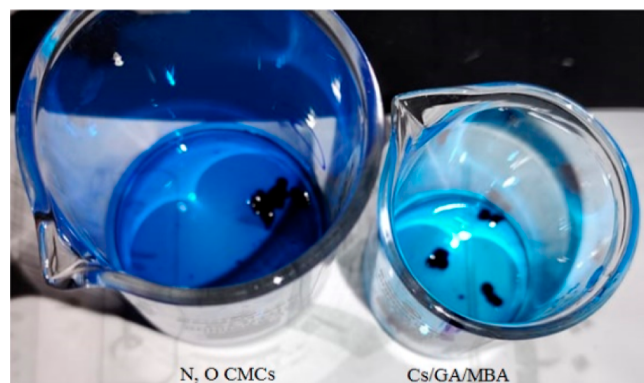

Figure 7. Decolorization of MB solution by N,O CMCs, and Cs/GA/MBA under optimized conditions.

Table 5. AFM Data of Dry and MB-Loaded Sorbents

sorbent	height of dry sorbent (nm)	the roughness of dye-free sorbents R_a (nm)	height of MB-loaded sorbent (nm)	the roughness of dye-loaded sorbents R_a (nm)
Cs/GA/MBA	6.56	23.11	45	35.34
Cs/GA/ECH	9.49	19.26	43	27.82
Cs-g-GA	3.76	15.72	34	21.67
N,O-CMCs	6.8	12.34	22	21.78

3.6.1. Monitoring the Dye Adsorption via AFM. Moreover, AFM can be effectively used in monitoring the adsorption process by comparing the surface features and the height of the surface before and after adsorption.[30,34] Figure 8 illustrates AFM images of dry and MB-loaded sorbents. Moreover, Gwyddion software was used to analyze the phase differentiation of the AFM images to show the different phases comprising the matrix. In all of the provided images, it can be seen that the adsorbed dye appears as white batches on the surface of the sorbent material. In some images, it can be noticed that the height of the dye-loaded sorbent is higher than that of the dry sorbent. This may be attributed to the process of dye uptake achieved by these sorbents being a combination of adsorption and absorption and the fact that some dye molecules are captured into the porous structure of the sorbent molecules. The outcomes of AFM are given in Table 5. Upon studying the topographies of the dry sorbents, one can detect some striations and convolutions in the AFM images of the cross-linked candidates which confirm the creation of network structure. This protocol fits our previous works[20,21] for employing the AFM in monitoring the adsorption process. Moreover, the roughness measurements of dye-free and dye-loaded sorbents were provided (as calculated from Flexaxiom software). It can be seen that the roughness values of the cross-linked derivatives are higher than those for uncross-linked ones which infers the formation of a porous structure. In addition, the roughness measurements increase with an increase in the adsorption capacities of the sorbent materials. This may be attributed to the adsorbed dyes accumulating on the surface as rough points.

3.6.2. Investigating the Dye Removal Process by the UV–Visible Absorption. The UV–visible absorption spectra are given in the range of 400−720 nm, Figure 9. After adsorption at different contact times, the concentration of four representative dyes decreased. The highest decrease in MB concentration was achieved by Cs/GA/MBA; then, the order of reduction was Cs/GA/ECH, Cs-g-GA and finally N,O CMCs.

3.7. Adsorption/Desorption Study. To investigate the reusability performance of the prepared sorbents, the sorbents were repeatedly washed with 1 N HCl solution and allowed to reabsorb the MB dye for 5 cycles.[47] Desorption with the acidic solution—not water—confirms strong electrostatic attraction[50−55] and hydrogen bonding formation between MB dye and the anionic groups in the sorbent molecules.[47] The data are listed in Figure 10. It can be seen that the percentage removal (% R) slightly reduced after five application cycles which infers superior workability of these sorbents toward MB dye.

3.8. Adsorption Capacities versus Other Adsorbents. A brief comparison of the adsorption capacities of some chitosan-based adsorbents toward MB is presented in Table 6. The data reveal that the prepared sorbents showed dye adsorption comparable to that of other chitosan-based sorbents. Moreover, the investigated sorbents were readily prepared with minimum preparation steps, making them excellent candidates for cationic dyes.

4. CONCLUSIONS

This work showed the potential of four chitosan-modified sorbents for the decolorization of the MB dye from an aqueous solution. The usage of cross-linked and non-cross-linked chitosan as green polymers in comparative research for eliminating MB dye is one of the material's advantages and inventions. The swelling performance of the prepared sorbents was verified under different application conditions, and the data
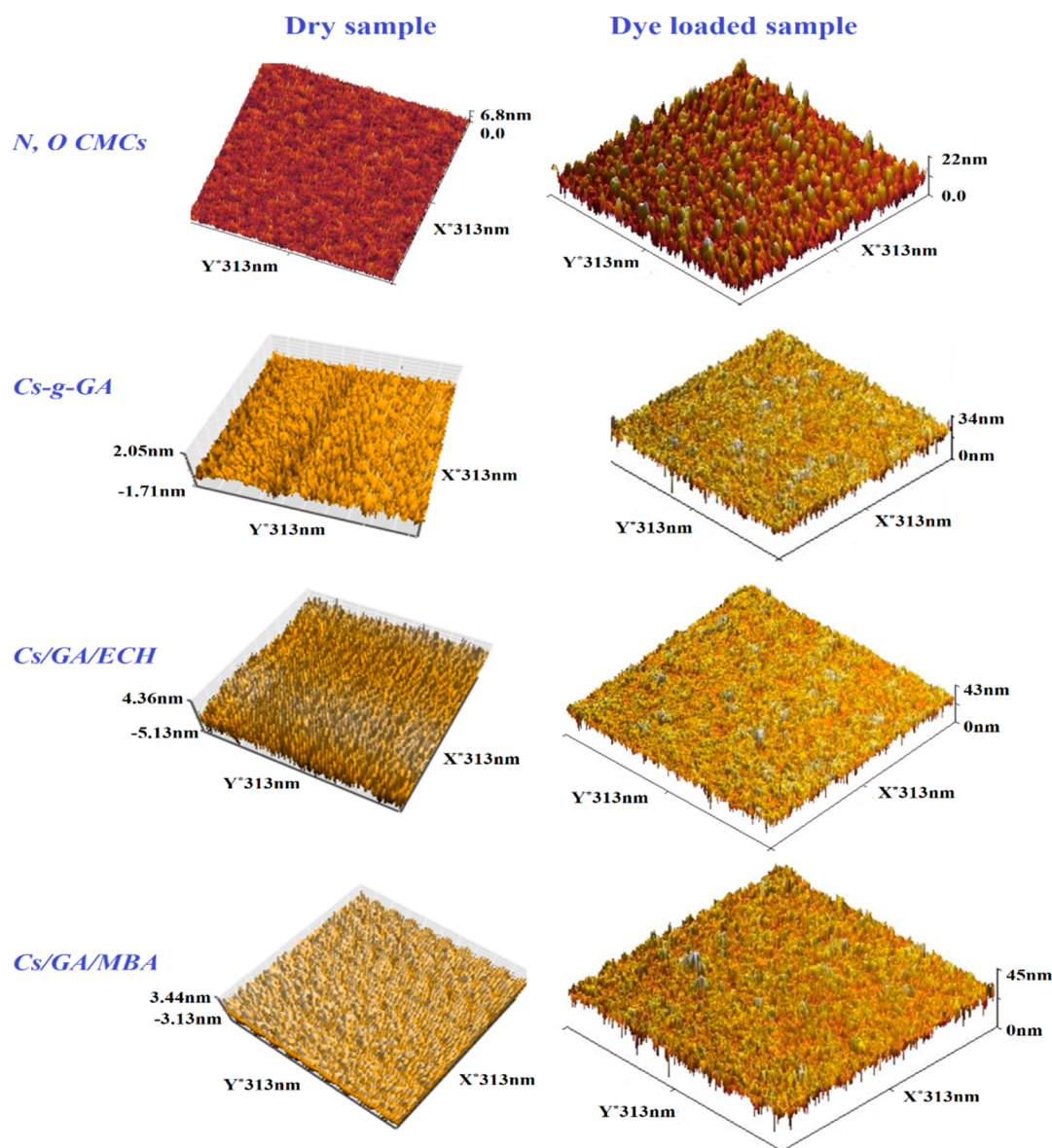
Figure 8. AFM images of the dry and dye-loaded chitosan sorbents.

Table 6. Adsorption Capacities of Various Adsorbents toward MB

the sorbent	q_e (mg·g) or percentage of removal	optimum conditions	references
chitin/CS-g-PAM	100%	pH = 8, sorbent concentration, 0.1 g/100 mL, initial dye concentration of 1.0 mg/L	36
chitosan/KIO$_3$	109 mg/g	pH = 8, 60 min, 30 °C, sorbent dose = 0.18 g	41
N,O-CMCTS	349 mg/g	N,O-CMCTS with the DS of 0.76, sample dose: 0.10 g/25 mL; pH: 8.0; temperature: 30 °C; equilibrium time: 60 min	42
cross-linked O-CM-chitosan hydrogel	434.8 mg/g	pH = 9, initial dye concentration = 50 ppm	47
magnetic chitosan and graphene oxide composite	95.16 mg/g	pH = 5.3, initial dye concentration = 60 mg/L	48
magnetic carboxymethyl chitosan aerogel	217.43 mg·g	pH = 8, 150 min, dye dosage = 0.3 g/L	49
N,O-CM/Cs	95.0898 mg/g	pH = 9, 150 min, dye dosage = 0.3 g/L	this work
Cs/GA	120.07 mg/g		
Cs/GA/ECH	220.097 mg/g		
Cs/GA/MBA	270.024 mg/g		

revealed that the maximum swelling was attained at pH = 9 and temperature 55 °C. Effects of critical parameters, including pH, initial MB concentrations, and the reaction temperature, were studied in batch experiments. The cross-linking technique creates more voids, which extends the adsorptive areas and increases the removal effectiveness of the MB dye. The cross-
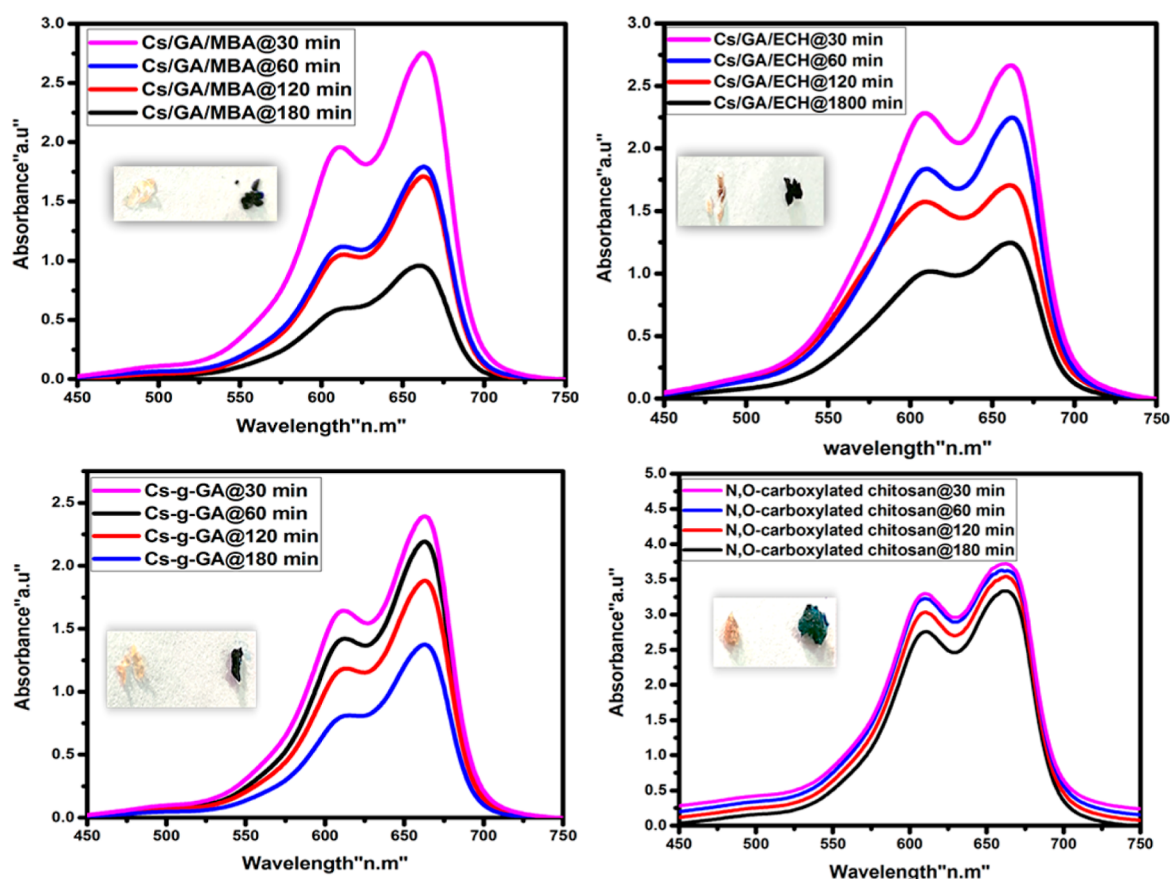
Figure 9. UV spectrum of the adsorption time of MB onto chitosan-based sorbents.
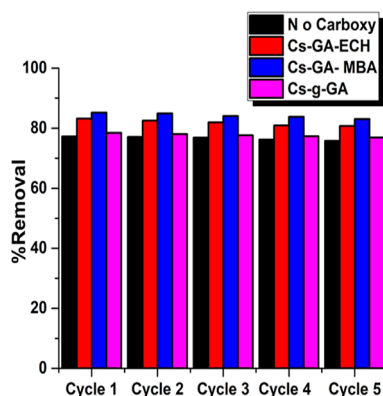

Figure 10. Sorption/desorption of the MB dye onto modified chitosan sorbents.

linked products (Cs/GA/MBA and Cs/GA/ECH) may absorb the MB dye even at higher temperatures. The kinetic studies of four kinetic models suggested that the decolorization process of MB is a chemisorption process, and it can be described by the second-order kinetic model for initial concentrations of 300 ppm of MB and can almost be completed in about 150 min. The adsorption process was also verified versus four adsorption isotherms, namely, Langmuir isotherm, Freundlich isotherm, Temkin isotherm, and Dubinin−Radushkevich isotherm. The R^2 data showed that the adsorption process best fits with the Langmuir isotherm model. Also, the decolorization efficiency of MB was strongly dependent on the pH of the solution, with maximum adsorption attained at pH 9.0 for all of the investigated sorbents. In addition, the removal process was

confirmed by AFM by comparing the height measurements of the dry and dye-loaded samples. The repeated decolorization of the water-soluble dye solution (five times) slightly affects the removal percentage. Finally, the removal capacities of the prepared sorbents toward MB were found comparable with other chitosan-based sorbents with advantages of feasibility and readiness of preparation methodologies applied in this paper.

■ ASSOCIATED CONTENT

Data Availability Statement

The raw data supporting the conclusions of this article will be made available by the authors upon reasonable request.

■ AUTHOR INFORMATION

Corresponding Author

Ahmed A. Farag − *Egyptian Petroleum Research Institute, Nasr City 11727 Cairo, Egypt;* ◉ orcid.org/0000-0002-9019-5635; Email: ahmedafm@yahoo.com

Authors

Manar El-Sayed Abdel-Raouf − *Egyptian Petroleum Research Institute, Nasr City 11727 Cairo, Egypt;* ◉ orcid.org/0000-0003-0718-2671

Reem Kamal Farag − *Egyptian Petroleum Research Institute, Nasr City 11727 Cairo, Egypt*

Mohamed Keshawy − *Egyptian Petroleum Research Institute, Nasr City 11727 Cairo, Egypt*

Alaa Abdel-Aziz − *Egyptian Petroleum Research Institute, Nasr City 11727 Cairo, Egypt*

Abdulraheim Hasan − *Egyptian Petroleum Research Institute, Nasr City 11727 Cairo, Egypt;* ● orcid.org/0000-0003-1918-7963

Author Contributions

Prof. Manar Abdel-raouf is the PI of the project, conceptualization, methodology, investigation, AFM data, writing—review and editing. Reem Kamal: data presentation, validation. Ahmad A. Farag: conceptualization, methodology, review and editing, publication. Mohamed keshawy: synthesis, experiment, data presentation. Alaa Abdel-aziz: experimental, AFM imaging, adsorption kinetics study. Abdulraheim Hasan: writing, editing, supervision.

Notes

The authors declare no competing financial interest.

■ REFERENCES

(1) Zango, Z. U.; Dennis, J. O.; Aljameel, A. I.; Usman, F.; Ali, M. K. M.; Abdulkadir, B. A.; Algessair, S.; Aldaghri, O. A.; Ibnaouf, K. H. Effective Removal of Methylene Blue from Simulated Wastewater Using ZnO-Chitosan Nanocomposites: Optimization, Kinetics, and Isotherm Studies. *Molecules* **2022**, *27* (15), 4746.

(2) Vakili, M.; Rafatullah, M.; Salamatinia, B.; Abdullah, A. Z.; Ibrahim, M. H.; Tan, K. B.; Gholami, Z.; Amouzgar, P. Application of Chitosan and Its Derivatives as Adsorbents for Dye Removal from Water and Wastewater: A Review. *Carbohydr. Polym.* **2014**, *113*, 115–130.

(3) Kyzas, G.; Bikiaris, D. Recent Modifications of Chitosan for Adsorption Applications: A Critical and Systematic Review. *Mar. Drugs* **2015**, *13* (1), 312–337.

(4) Imam, S.; Muhammad, A. I.; Babamale, H. F.; Zango, Z. U. Removal of Orange G Dye from Aqueous Solution by Adsorption: A Short Review. *J. Environ. Treat. Technol.* **2020**, *9* (1), 318–327.

(5) Zhai, L.; Bai, Z.; Zhu, Y.; Wang, B.; Luo, W. Fabrication of Chitosan Microspheres for Efficient Adsorption of Methyl Orange. *Chin. J. Chem. Eng.* **2018**, *26* (3), 657–666.

(6) Zango, Z. U. Cationic Dyes Removal Using Low-Cost Banana Peel Biosorbent. *Am. J. Mater. Sci.* **2018**, *8*, 32–38.

(7) Pietrelli, L.; Francolini, I.; Piozzi, A. Dyes Adsorption from Aqueous Solutions by Chitosan. *Sep. Sci. Technol.* **2015**, *50* (8), 1101–1107.

(8) Ge, Y.-M.; Zhao, X.-F.; Xu, J.-H.; Liu, J.-Z.; Yang, J.-S.; Li, S.-J. Recyclable Magnetic Chitosan Microspheres with Good Ability of Removing Cationic Dyes from Aqueous Solutions. *Int. J. Biol. Macromol.* **2021**, *167*, 1020–1029.

(9) Oladoye, P. O.; Ajiboye, T. O.; Omotola, E. O.; Oyewola, O. J. Methylene Blue Dye: Toxicity and Potential Elimination Technology from Wastewater. *Results Eng.* **2022**, *16*, 100678.

(10) Ahmad, M. A.; Eusoff, M. A.; Oladoye, P. O.; Adegoke, K. A.; Bello, O. S. Optimization and Batch Studies on Adsorption of Methylene Blue Dye Using Pomegranate Fruit Peel Based Adsorbent. *Chem. Data Collect.* **2021**, *32*, 100676.

(11) Amer, A.; Sayed, G. H.; Ramadan, R. M.; Rabie, A. M.; Negm, N. A.; Farag, A. A.; Mohammed, E. A. Assessment of 3-Amino-1H-1,2,4-Triazole Modified Layered Double Hydroxide in Effective Remediation of Heavy Metal Ions from Aqueous Environment. *J. Mol. Liq.* **2021**, *341*, 116935.

(12) Guillen, G. R.; Pan, Y.; Li, M.; Hoek, E. M. V. Preparation and Characterization of Membranes Formed by Nonsolvent Induced Phase Separation: A Review. *Ind. Eng. Chem. Res.* **2011**, *50* (7), 3798–3817.

(13) Hashem, A. H.; Saied, E.; Hasanin, M. S. Green and Ecofriendly Bio-Removal of Methylene Blue Dye from Aqueous Solution Using Biologically Activated Banana Peel Waste. *Sustainable Chem. Pharm.* **2020**, *18*, 100333.

(14) Wahab, M. M. A.; Sayed, G. H.; Ramadan, R. M.; Mady, A. H.; Rabie, A. M.; Farag, A. A.; Negm, N. A.; Mohamed, E. A. Synergistic Effects of Graphene Oxide Grafted with Barbituric Acid Nanocomposite for Removal of Heavy Metals from Aqueous Solution. *Nanotechnol. Environ. Eng.* **2023**, *8*, 347−359.

(15) Hama Aziz, K. H.; Mahyar, A.; Miessner, H.; Mueller, S.; Kalass, D.; Moeller, D.; Khorshid, I.; Rashid, M. A. M. Application of a Planar Falling Film Reactor for Decomposition and Mineralization of Methylene Blue in the Aqueous Media via Ozonation, Fenton, Photocatalysis and Non-Thermal Plasma: A Comparative Study. *Process Saf. Environ. Prot.* **2018**, *113*, 319−329.

(16) Javaid, R.; Qazi, U. Y. Catalytic Oxidation Process for the Degradation of Synthetic Dyes: An Overview. *Int. J. Environ. Res. Public Health* **2019**, *16* (11), 2066.

(17) Hoc Thang, N.; Sy Khang, D.; Duy Hai, T.; Thi Nga, D.; Dinh Tuan, P. Methylene Blue Adsorption Mechanism of Activated Carbon Synthesised from Cashew Nut Shells. *RSC Adv.* **2021**, *11* (43), 26563−26570.

(18) Jawad, A. H.; Abdulhameed, A. S.; Hanafiah, M. A. K. M.; Alothman, Z. A.; Khan, M. R.; Surip, S. N. Numerical Desirability Function for Adsorption of Methylene Blue Dye by Sulfonated Pomegranate Peel Biochar: Modeling, Kinetic, Isotherm, Thermodynamic, and Mechanism Study. *Korean J. Chem. Eng.* **2021**, *38* (7), 1499−1509.

(19) Farag, A. A.; Gafar Afif, A.; Salih, S. A.; Altalhi, A. A.; Mohamed, E. A.; Mohamed, G. G. Highly Efficient Elimination of Pb^{+2} and Al^{+3} Metal Ions from Wastewater Using Graphene Oxide/3,5-Diaminobenzoic Acid Composites: Selective Removal of Pb2+from Real Industrial Wastewater. *ACS Omega* **2022**, *7*, 38347−38360.

(20) Sayed, A.; Mazrouaa, A. M.; Mohamed, M. G.; Abdel-Raouf, M. E. S. Green Synthesis of Chitosan/Erythritol/Graphene Oxide Composites for Simultaneous Removal of Some Toxic Species from Simulated Solution. *Environ. Sci. Pollut. Res.* **2023**, *30*, 25903−25919.

(21) Mahmoud, G. A.; Sayed, A.; Abdel-raouf, M. E.; Danial, M. Y. F.; Amin, A. Efficient Removal of Cr^{6+} from Aqueous Solutions Using Chitosan/Na alginate Bio based Nanocomposite Hydrogel. *J. Appl. Polym. Sci.* **2023**, *140* (21), No. e53886, DOI: 10.1002/app.53886.

(22) Ahmed, H. A.; Altalhi, A. A.; Elbanna, S. A.; El-Saied, H. A.; Farag, A. A.; Negm, N. A.; Mohamed, E. A. Effect of Reaction Parameters on Catalytic Pyrolysis of Waste Cooking Oil for Production of Sustainable Biodiesel and Biojet by Functionalized Montmorillonite/Chitosan Nanocomposites. *ACS Omega* **2022**, *7* (5), 4585−4594.

(23) El-araby, A.; El Ghadraoui, L.; Errachidi, F. Physicochemical Properties and Functional Characteristics of Ecologically Extracted Shrimp Chitosans with Different Organic Acids during Demineralization Step. *Molecules* **2022**, *27* (23), 8285.

(24) Aranaz, I.; Alcántara, A. R.; Civera, M. C.; Arias, C.; Elorza, B.; Heras Caballero, A.; Acosta, N. Chitosan: An Overview of Its Properties and Applications. *Polymers* **2021**, *13* (19), 3256.

(25) Pal, P.; Pal, A.; Nakashima, K.; Yadav, B. K. Applications of Chitosan in Environmental Remediation: A Review. *Chemosphere* **2021**, *266*, 128934.

(26) Kou, S. G.; Peters, L.; Mucalo, M. Chitosan: A Review of Molecular Structure, Bioactivities and Interactions with the Human Body and Micro-Organisms. *Carbohydr. Polym.* **2022**, *282*, 119132.

(27) El Knidri, H.; Belaabed, R.; Addaou, A.; Laajeb, A.; Lahsini, A. Extraction, Chemical Modification and Characterization of Chitin and Chitosan. *Int. J. Biol. Macromol.* **2018**, *120*, 1181−1189.

(28) Kou, S. G.; Peters, L. M.; Mucalo, M. R. Chitosan: A Review of Sources and Preparation Methods. *Int. J. Biol. Macromol.* **2021**, *169*, 85−94.

(29) Al-Manhel, A. J.; Al-Hilphy, A. R. S.; Niamah, A. K. Extraction of Chitosan, Characterisation and Its Use for Water Purification. *J. Saudi Soc. Agric. Sci.* **2018**, *17* (2), 186−190.

(30) El-Sayed Abdel-Raouf, M.; Kamal, R. S.; Hegazy, D. E.; Sayed, A. Gamma Irradiation Synthesis of Carboxymethyl Chitosan-Nanoclay Hydrogel for the Removal of Cr(VI) and Pb(II) from Aqueous Media. *J. Inorg. Organomet. Polym. Mater.* **2023**, *33* (4), 895−913.

(31) Chandra, D.; Molla, M. T. H.; Bashar, M. A.; Islam, M. S.; Ahsan, M. S. Chitosan-Based Nano-Sorbents: Synthesis, Surface Modification, Characterisation and Application in Cd (II), Co (II), Cu (II) and Pb (II) Ions Removal from Wastewater. *Sci. Rep.* **2023**, *13* (1), 6050.

(32) Benettayeb, A.; Seihoub, F. Z.; Pal, P.; Ghosh, S.; Usman, M.; Chia, C. H.; Usman, M.; Sillanpää, M. Chitosan Nanoparticles as Potential Nano-Sorbent for Removal of Toxic Environmental Pollutants. *Nanomaterials* **2023**, *13* (3), 447.

(33) Li, Y.; Zhou, Y.; Nie, W.; Song, L.; Chen, P. Highly Efficient Methylene Blue Dyes Removal from Aqueous Systems by Chitosan Coated Magnetic Mesoporous Silica Nanoparticles. *J. Porous Mater.* **2015**, *22* (5), 1383−1392.

(34) Abdel-Raouf, M. E.; Farag, R. K.; Farag, A. A.; Keshawy, M.; Abdel-Aziz, A.; Hasan, A. Chitosan-Based Architectures as an Effective Approach for the Removal of Some Toxic Species from Aqueous Media. *ACS Omega* **2023**, *8* (11), 10086−10099.

(35) Sayed, A.; Mohamed, M. M.; Abdel-raouf, M. E.-S.; Mahmoud, G. A. Radiation Synthesis of Green Nanoarchitectonics of Guar Gum-Pectin/Polyacrylamide/Zinc Oxide Superabsorbent Hydrogel for Sustainable Agriculture. *J. Inorg. Organomet. Polym. Mater.* **2022**, *32* (12), 4589−4600.

(36) Labidi, A.; Salaberria, A.; Fernandes, S.; Labidi, J.; Abderrabba, M. Functional Chitosan Derivative and Chitin as Decolorization Materials for Methylene Blue and Methyl Orange from Aqueous Solution. *Materials* **2019**, *12* (3), 361.

(37) Uddin, M. T.; Rahman, M. A.; Rukanuzzaman, M.; Islam, M. A. A Potential Low Cost Adsorbent for the Removal of Cationic Dyes from Aqueous Solutions. *Appl. Water Sci.* **2017**, *7* (6), 2831−2842.

(38) Perez Bravo, J. J.; François, N. J. Chitosan/Starch Matrices Prepared by Ionotropic Gelation: Rheological Characterization, Swelling Behavior and Potassium Nitrate Release Kinetics. *J. Polym. Environ.* **2020**, *28* (10), 2681−2690.

(39) El-Dossoki, F.; Abedelhady, S.; Abedalhmeed, M.; Abdel-Raouf, M.; Ali, A. Micellization Properties, Molal Volume and Polarizability of Newly Synthesized Gemini-Cationic Surfactants. *Egypt. J. Chem.* **2022**, *65* (6), 585−599.

(40) Abukhadra, M. R.; Adlii, A.; Bakry, B. M. Green Fabrication of Bentonite/Chitosan@cobalt Oxide Composite (BE/CH@Co) of Enhanced Adsorption and Advanced Oxidation Removal of Congo Red Dye and Cr (VI) from Water. *Int. J. Biol. Macromol.* **2019**, *126*, 402−413.

(41) Pam, A. A.; Ande, S.; Eneji, I. S.; Sha'Ato, R. Sorption of Methylene Blue on Iodate-Chitosan Assembled Composite from Aqueous Solution. *Desalin. Water Treat.* **2019**, *164*, 388−395.

(42) Jawad, A. H.; Mubarak, N. S. A.; Sabar, S. Adsorption and Mechanism Study for Reactive Red 120 Dye Removal by Cross-Linked Chitosan-Epichlorohydrin Biobeads. *Desalin. Water Treat.* **2019**, *164*, 378−387.

(43) Wang, L.; Li, Q.; Wang, A. Adsorption of Cationic Dye on N,O-Carboxymethyl-Chitosan from Aqueous Solutions: Equilibrium, Kinetics, and Adsorption Mechanism. *Polym. Bull.* **2010**, *65* (9), 961−975.

(44) Elhadj, M.; Samira, A.; Mohamed, T.; Djawad, F.; Asma, A.; Djamel, N. Removal of Basic Red 46 Dye from Aqueous Solution by Adsorption and Photocatalysis: Equilibrium, Isotherms, Kinetics, and Thermodynamic Studies. *Sep. Sci. Technol.* **2020**, *55* (5), 867−885.

(45) Sayed, A.; Mahmoud, G. A.; Said, H.; Diab, A. A. Character-ization and Optimization of Magnetic Gum-PVP/SiO2 Nano-composite Hydrogel for Removal of Contaminated Dyes. *Mater. Chem. Phys.* **2022**, *280*, 125731.

(46) Alharby, N. F.; Almutairi, R. S.; Mohamed, N. A. Adsorption Behavior of Methylene Blue Dye by Novel CrossLinked O-CM-Chitosan Hydrogel in Aqueous Solution: Kinetics, Isotherm and Thermodynamics. *Polymers* **2021**, *13* (21), 3659.

(47) Farag, R. K.; El-Saeed, S. M.; Abdel-Raouf, M. E. Synthesis and Investigation of Hydrogel Nanoparticles Based on Natural Polymer for Removal of Lead and Copper(II) Ions. *Desalin. Water Treat.* **2016**, *57* (34), 16150−16160.

(48) Fan, L.; Luo, C.; Li, X.; Lu, F.; Qiu, H.; Sun, M. Fabrication of Novel Magnetic Chitosan Grafted with Graphene Oxide to Enhance Adsorption Properties for Methyl Blue. *J. Hazard. Mater.* **2012**, *215−216*, 272−279.

(49) Lei, C.; Wen, F.; Chen, J.; Chen, W.; Huang, Y.; Wang, B. Mussel-Inspired Synthesis of Magnetic Carboxymethyl Chitosan Aerogel for Removal Cationic and Anionic Dyes from Aqueous Solution. *Polymer* **2021**, *213*, 123316.

(50) Farag, A. A.; Abdallah, H. E.; Badr, E. A.; Mohamed, E. A.; Ali, A. I.; El-Etre, A. Y. The Inhibition Performance of Morpholinium Derivatives on Corrosion Behavior of Carbon Steel in the Acidized Formation Water: Theoretical, Experimental and Biocidal Evaluations. *J. Mol. Liq.* **2021**, *341*, 117348.

(51) Hashem, H. E.; Farag, A. A.; Mohamed, E. A.; Azmy, E. M. Experimental and Theoretical Assessment of Benzopyran Compounds as Inhibitors to Steel Corrosion in Aggressive Acid Solution. *J. Mol. Struct.* **2022**, *1249*, 131641.

(52) Farag, A. A. Oil-in-Water Emulsion of a Heterocyclic Adduct as a Novel Inhibitor of API X52 Steel Corrosion in Acidic Solution. *Corros. Rev.* **2018**, *36* (6), 575−588.

(53) Farag, A. A.; Badr, E. A. Non-Ionic Surfactant Loaded on Gel Capsules to Protect Downhole Tubes from Produced Water in Acidizing Oil Wells. *Corros. Rev.* **2020**, *38* (2), 151−164.

(54) Shaban, S. M.; Badr, E. a.; Shenashen, M.; Farag, A. Fabrication and Characterization of Encapsulated Gemini Cationic Surfactant as Anticorrosion Material for Carbon Steel Protection in Down-Hole Pipelines. *Environ. Technol. Innovation* **2021**, *23*, 101603.

(55) Shaban, M. M.; Negm, N.; Farag, R.; Fadda, A.; Gomaa, A. E.; Farag, A.; Migahed, M. Anti-Corrosion, Antiscalant and Anti-Microbial Performance of Some Synthesized Trimeric Cationic Imidazolium Salts in Oilfield Applications. *J. Mol. Liq.* **2022**, *351*, 118610.